How to cite: *Angew. Chem. Int. Ed.* **2022**, *61*, e202112511
International Edition: doi.org/10.1002/anie.202112511
German Edition: doi.org/10.1002/ange.202112511

Layered Double Hydroxides

$Mo_3S_{13}^{2-}$ Intercalated Layered Double Hydroxide: Highly Selective Removal of Heavy Metals and Simultaneous Reduction of Ag^+ Ions to Metallic Ag^0 Ribbons

Lixiao Yang[+], Linxia Xie[+], Menglin Chu[+], Hui Wang, Mengwei Yuan, Zihuan Yu, Chaonan Wang, Huiqin Yao,* Saiful M. Islam, Keren Shi, Dongpeng Yan, Shulan Ma,* and Mercouri G. Kanatzidis**

Abstract: *We demonstrate a new material by intercalating $Mo_3S_{13}^{2-}$ into Mg/Al layered double hydroxide (abbr. Mo_3S_{13}-LDH), exhibiting excellent capture capability for toxic Hg^{2+} and noble metal silver (Ag). The as-prepared Mo_3S_{13}-LDH displays ultra-high selectivity of Ag^+, Hg^{2+} and Cu^{2+} in the presence of various competitive ions, with the order of $Ag^+ > Hg^{2+} > Cu^{2+} > Pb^{2+} \geq Co^{2+}$, Ni^{2+}, Zn^{2+}, Cd^{2+}. For Ag^+ and Hg^{2+}, extremely fast adsorption rates ($\approx 90\,\%$ within 10 min, $> 99\,\%$ in 1 h) are observed. Much high selectivity is present for Ag^+ and Cu^{2+}, especially for trace amounts of Ag^+ (≈ 1 ppm), achieving a large separation factor ($SF_{Ag/Cu}$) of ≈ 8000 at the large Cu/Ag ratio of 520. The overwhelming adsorption capacities for Ag^+ ($q_m^{Ag} = 1073\ mg\,g^{-1}$) and Hg^{2+} ($q_m^{Hg} = 594\ mg\,g^{-1}$) place the Mo_3S_{13}-LDH at the top of performing sorbent materials. Most importantly, Mo_3S_{13}-LDH captures Ag^+ via two paths: a) formation of Ag_2S due to Ag-S complexation and precipitation, and b) reduction of Ag^+ to metallic silver (Ag^0). The Mo_3S_{13}-LDH is a promising material to extract low-grade silver from copper-rich minerals and trap highly toxic Hg^{2+} from polluted water.*

Introduction

The removal of toxic heavy metal ions from aquatic ecosystems and industrial water is a key environmental problem. The release of industrial waste effluents containing heavy metal ions (Hg^{2+}, Pb^{2+}, etc.) into water bodies has toxic effects on human beings, such as the neurological impairment and central nervous system damage.[1] It is necessary to remove these toxic heavy metal ions from the polluted water environments. In addition, silver is a precious metal as well as critical in modern electronics, medicine and chemical catalysis.[2] Indeed, Nanotechnology Consumer Product Inventory of Woodrow Wilson Institute (2016) lists more than 350 manufacturer-identified products that contain silver nanoparticles.[3] However, the noble metal silver is generally extracted from low-abundance silver-bearing minerals accompanied by a variety of other metals such as Zn, Pb, and Cu. Thus, it is of great significance to extract precious Ag selectively at low cost.

Various materials including zeolites, activated carbon, polymers, biomaterials, and sorption resins have been investigated to remove or trap the heavy metal ions. Based on the Lewis acid-base theory, the sulfides as soft base have high affinity with the soft-acidic heavy metal ions.[4] Sulfur-based crystalline materials such as $K_{2x}Mn_xSn_{3-x}S_6$ (KMS-1),[5] $H_{2x}MnSn_{3-x}S_6$ (LHMS),[6] $K_{2x}Mg_xSn_{3-x}S_6$ (KMS-2)[7] and $K_{2x}Sn_{4-x}S_{8-x}$ (KTS-3),[8] and amorphous $A_{2-x}A'_xSnSb_2S_6$ (A = Na, Cs, A′ = K)[9] are employed to remediate the heavy metal polluted water. $Mo_3S_{13}^{2-}$ is a kind of molybdenum sulfides composed of various types of sulfur atoms located in the edges.[10] However, due to the low solubility of $(NH_4)_2Mo_3S_{13}$ crystals in water, adsorption sites of $Mo_3S_{13}^{2-}$ can not be exposed to a great extent, which weakens the capture capacity. In order to enhance the functionality of this cluster toward metal ion binding, we prepared polypyrrole-Mo_3S_{13} (Ppy-Mo_3S_{13}) and found it exhibited a maximum uptake of $408\ mg\,g^{-1}$ for Ag^+, and the Mo^{4+} in $Mo_3S_{13}^{2-}$ contributed primarily to the reduction of Ag^+ to Ag^0 metals.[11]

Layered double hydroxides (LDHs) are a famous class of low-cost sorbents concluding positively-charged layers and

[*] L. X. Yang,[+] L. X. Xie,[+] M. L. Chu,[+] H. Wang, Dr. M. W. Yuan, Z. H. Yu, C. N. Wang, Prof. D. P. Yan, Prof. S. L. Ma
Beijing Key Laboratory of Energy Conversion and Storage Materials, College of Chemistry, Beijing Normal University
Beijing 100875 (China)
E-mail: mwyuan@mail.bnu.edu.cn
mashulan@bnu.edu.cn

Prof. H. Q. Yao
School of Basic Medical Sciences, Ningxia Medical University
Yinchuan 750004 (China)
E-mail: huiqin_yao@163.com

Dr. S. M. Islam, Prof. M. G. Kanatzidis
Department of Chemistry, Northwestern University
2145 Sheridan Road, Evanston, IL 60208 (USA)
E-mail: m-kanatzidis@northwestern.edu

Dr. S. M. Islam
Department of chemistry, Physics and Atmospheric Sciences, Jackson State University
Jackson, MS 39217 (USA)

Dr. K. R. Shi
State Key Laboratory of High-efficiency Utilization of Coal and Green Chemical Engineering, Ningxia University
Yinchuan 750021 (China)

[+] These authors contributed equally to this work.

Supporting information and the ORCID identification number(s) for the author(s) of this article can be found under: https://doi.org/10.1002/anie.202112511.

counter-anions in interlayers. The intercalation and ion-exchange capability of the LDHs endow them many characteristics applied as adsorbents,[12] catalysts,[13] supercapacitors,[14] and etc. When LDH interlayers are functionalized with thioanions, the resulting products exhibited excellent capture capacity for heavy ions, due to strong M-S affinity.[15] We previously introduced S_x^{2-} and MoS_4^{2-} into LDH galleries to construct S_x-LDH[16] and MoS_4-LDH,[17] displaying effective capture for heavy metals (UO_2^{2+}, Ag^+, Cu^{2+}, and Hg^{2+}). The MoS_4-LDH also presented excellent uptake for toxic oxoanions of As^{3+}, As^{5+}, Cr^{6+},[18] and simultaneous removals of Se^{4+}/Se^{6+} oxoanions and metal cations such as Cu^{2+}, Cd^{2+} and Hg^{2+}.[19] As for the role of LDH layers, Kim et al. gave high evaluation for our S_x-LDH in the review paper,[20] in which they explained the insertion of polysulfides ensures their uniform dispersion in the gallery of LDH, so that the metal ions could be captured by every polysulfide ion.[20]

In this work, we intercalate the $Mo_3S_{13}^{2-}$ into the MgAl-LDH to obtain a new material of Mo_3S_{13}-LDH and study its sorption capability towards heavy metal ions. The as-prepared Mo_3S_{13}-LDH presents extremely high adsorption capacities of Ag^+ (1073 mg g^{-1}) and Hg^{2+} (594 mg g^{-1}) and much large selectivity. Most importantly, the Mo_3S_{13}-LDH can: a) use its sulfide ions to form Ag_2S and b) reduce Ag^+ to Ag^0 ribbons, attributed to the reducibility of S_2^{2-} and Mo^{4+} in $Mo_3S_{13}^{2-}$. This work highlights an effective and functional sorbent to exhibit exceptional selectivity for heavy metals and silver ion.

Results and Discussion

Characterization of Mo_3S_{13}-LDH

The MgAl-Mo_3S_{13}-LDH (abbr. Mo_3S_{13}-LDH) was prepared via ion-exchange of $Mo_3S_{13}^{2-}$ with NO_3^- in MgAl-NO_3-LDH. X-ray diffraction (XRD) measurements verify the formation of Mo_3S_{13}-LDH. The XRD pattern of $(NH_4)_2Mo_3S_{13}$ (Figure 1 A-a) is consistent with reported.[10] The NO_3-LDH has a basal spacing (d_{basal}) of 0.89 nm (Figure 1 A-b). In Mo_3S_{13}-LDH, the enlarged d_{basal} of 0.91 nm demonstrates insertion of the large anionic cluster of $Mo_3S_{13}^{2-}$ (Figure 1 A-c). The peak at $d = 0.15$ nm assigned to (110) plane of LDH indicates the retention of brucite layers, that is, a topotactic ion-exchange. Simultaneously, typical diffractions of $(NH_4)_2Mo_3S_{13}$ as found in Figure 1 A-a disappear, suggesting a pure Mo_3S_{13}-LDH phase is obtained. In infrared spectroscopy (IR) spectra of Mo_3S_{13}-LDH (Figure 1 B), the NO_3^- band ($\approx$1384 cm^{-1}) is markedly weakened, consistent with partial exchange of NO_3^- with $Mo_3S_{13}^{2-}$, as found in the composition of $Mg_{0.64}Al_{0.34}(OH)_2(Mo_3S_{13})_{0.053}(NO_3)_{0.20}\cdot 0.61\,H_2O$ (Table S1). The presence of $Mo_3S_{13}^{2-}$ is verified by Raman spectra (Figure 1 C). In $(NH_4)_2Mo_3S_{13}$ (Figure 1 C-a), the peaks at 550, 513, 454, 387–285 cm^{-1} are attributed to vibrations of ν(S-S)$_{term}$, ν(S-S)$_{bri}$, ν(Mo$_3$-S), and ν(Mo-S),[21] while in Mo_3S_{13}-LDH (Figure 1 C-b), corresponding stretching bands appear at 554, 517, 458, 388–285 cm^{-1}, for which the blue-shift arises from Mo–S···HO bonding of $Mo_3S_{13}^{2-}$ with LDH hydroxides. Scanning electron microscope (SEM) image (Figure 1 D) demonstrates the hexagonal

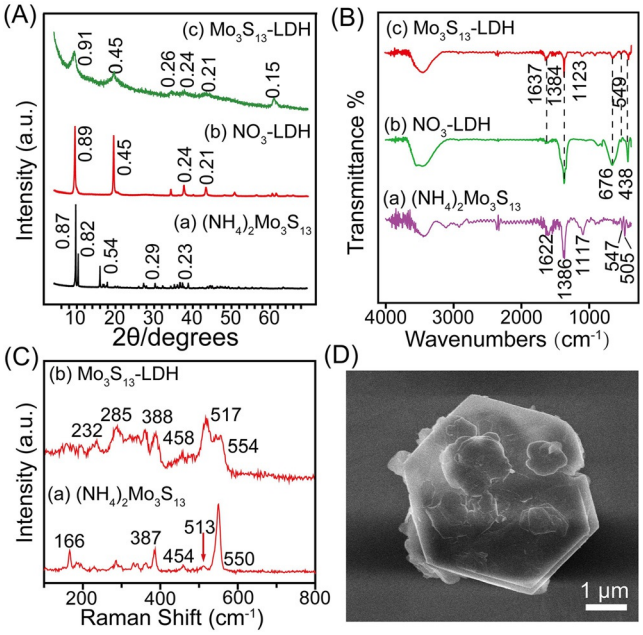

Figure 1. A) XRD patterns and B) IR spectra of $(NH_4)_2Mo_3S_{13}$, NO_3-LDH, and Mo_3S_{13}-LDH; C) Raman spectra of $(NH_4)_2Mo_3S_{13}$ and Mo_3S_{13}-LDH; D) SEM image of Mo_3S_{13}-LDH.

crystals of Mo_3S_{13}-LDH, as observed for the NO_3-LDH precursor.[16a]

Adsorption toward Heavy Metal Ions

To study competitive capture of metal ions by Mo_3S_{13}-LDH, eight ions of Ag^+, Pb^{2+}, Cd^{2+}, Hg^{2+}, Co^{2+}, Ni^{2+}, Cu^{2+}, and Zn^{2+} (pair anions are nitrate) were mixed together in a single solution ($\approx$10 ppm for each ion). From Table 1, after 24 h contact, the concentrations of Cu^{2+}, Hg^{2+} and Ag^+ were reduced to 0.15, 0.03 and 0.001 ppm, depicting highly efficient uptake (>99.5 %) toward Hg^{2+} and Ag^+. There were observed acceptable capture (>98 %) for Cu^{2+} and moderate trapping (57.6 %) for Pb^{2+}, in comparison to poor removals for Co^{2+}, Ni^{2+}, Cd^{2+} and Zn^{2+}, giving selectivity order of Co^{2+}, Ni^{2+}, $Cd^{2+} < Zn^{2+} \ll Pb^{2+} < Cu^{2+} < Hg^{2+} < Ag^+$. This difference not only relies on the soft and hard Lewis acid-base theory, but also is affected by the steric hindrance of the

Table 1: Adsorption data of Mo_3S_{13}-LDH towards the mixture of eight ions.[a]

Ion	C_0 [ppm]	C_f [ppm]	Removal [%]	K_d [mL g^{-1}]
Co^{2+}	10.5	9.80	6.67	71
Ni^{2+}	10.6	9.81	7.45	81
Cu^{2+}	10.7	0.15	98.60	7.0×10^4
Zn^{2+}	10.5	9.67	7.90	86
Ag^+	10.9	$\leq$0.001	$\geq$99.99	5.4×10^7
Pb^{2+}	10.5	4.45	57.62	1.4×10^3
Cd^{2+}	10.3	9.50	7.77	84
Hg^{2+}	10.8	0.03	99.72	3.6×10^5

[a] Contact time: 24 h, $V = 20$ mL, $m = 0.02$ g, $V/m = 1000$ mL g^{-1}, pH: 2.42–4.18.

hydrated metal ions coordinated by water. In aqueous solutions, Co^{2+}, Ni^{2+}, Cu^{2+}, and Zn^{2+} normally exist in the form of six coordination structure, but for Cu^{2+}, due to the Jahn–Teller effect, a square planar structure of $Cu(H_2O)_4^{2+}$ would dominate, and d_{z^2} orbital presents the smaller steric hindrance. In addition, Cu^{2+} is likely reduced to Cu^{+} which is considerably softer than Cu^{2+}. The Cd^{2+} is larger and adopts an octahedral coordinated motif of $Cd(H_2O)_6^{2+}$, and has a larger steric hindrance due to six coordination. Pb^{2+} mainly exists in the form of $Pb(H_2O)_6^{2+}$, forming an octahedral configuration, resulting in clear steric hindrance. Therefore, the softer Cu^{+} is selected first over Cd^{2+} and Pb^{2+}. Even though Pb^{2+} and Cd^{2+} adopt similar six coordination, Pb^{2+} is much softer than Cd^{2+}, so binding ability of soft base S to Pb^{2+} is stronger than to Cd^{2+}. Additionally, hydrated Ag^{+} is linear $Ag(H_2O)_2^{+}$ and Hg^{2+} is anhydrous or weakly hydrated, and they are also very soft Lewis acids, leading to good uptake. This matches well with S_x-LDH[16a] and MoS_4-LDH.[17]

Table 2: Sorption data of Mo_3S_{13}-LDH towards Cu^{2+}/Ag^{+} mixture.

Cu/Ag (ppm ratio)	Cu/Ag (molar ratio)	C_0 [ppm]	C_f [ppm]	Removal [%]	K_d [mL g^{-1}]	$SF_{Ag/Cu}$
0.5:1[a]	0.84	Cu: 0.50	<0.001	>99.80	4.99×10^5	2.14
		Ag: 1.07	<0.001	>99.91	1.07×10^6	
10:1[b]	16.8	Cu^{2+}: 8.80	0.57	93.54	1.45×10^4	80.69
		Ag^{+}: 1.17	<0.001	>99.91	1.17×10^6	
25:1[c]	42	Cu^{2+}: 24.6	9.53	61.30	1.58×10^3	772.2
		Ag^{+}: 1.22	<0.001	>99.92	1.22×10^6	
50:1[d]	84	Cu^{2+}: 49.1	25.6	47.95	4.80×10^2	2750
		Ag^{+}: 1.33	<0.001	>99.92	1.32×10^6	
100:1[e]	168	Cu^{2+}: 97.8	64.5	34.02	3.40×10^2	4176
		Ag^{+}: 1.42	<0.001	>99.93	1.42×10^6	
520:1[f]	874	Cu^{2+}: 521	462	11.38	1.28×10^2	7969
		Ag^{+}: 1.02	<0.001	>99.90	$>1.02\times10^6$	

[a] pH: 6.23→5.33, [b] pH: 5.87→5.11, [c] pH: 5.74→4.73, [d] pH: 5.47→4.57, [e] pH: 5.06→4.94, [f] pH: 4.64→4.04.

Generally, K_d values of $\approx10^4$–10^5 mL g^{-1} can be seen as good sorbents.[5,22] From Table 1, the K_d^{Ag} of 5.4×10^7 mL g^{-1} is higher than KMS-2 (1.2×10^3–3.6×10^5 mL g^{-1}), and close to those of MoS_4-LDH (1.4×10^7 mL g^{-1})[17] and S_x-LDH (4.1×10^5–6.8×10^7 mL g^{-1}).[16a] The K_d^{Hg} is 3.6×10^5 mL g^{-1}, matching well with commercial resins ($\approx10^4$–5.1×10^5 mL g^{-1}).[23] All these reflect the strong potential of Mo_3S_{13}-LDH as a superior adsorbent for capturing these heavy metals. Given the high selectivity of Mo_3S_{13}-LDH for Ag^{+}, Hg^{2+}, and Cu^{2+}, we conducted their separate adsorption (Table S2). For Ag^{+}, within 24 h, 99.99% removal was achieved, and 10 ppm concentration was decreased to <1 ppb. For Hg^{2+} and Cu^{2+}, 99.93% and 99.86% removals were reached, giving final concentrations of 6 ppb and 10 ppb, respectively. For Cu^{2+}, in the absence of competitive ions, we observed ≈10 fold higher ($=6.99\times10^5/7.0\times10^4$) K_d^{Cu} compared with the mixture of ions.

Considering that in many natural ores Ag^{+} ions occur in Cu-rich environments, we tested whether Mo_3S_{13}-LDH could extract silver from solutions with very high Cu^{2+} concentrations. Because such a challenging problem is often encountered in mining operation of precious metals, quick and low-cost separation of Cu and Ag is significant. From Table 2, at ≈1 ppm Ag^{+} and Cu^{2+} concentrations from 0.5 to 520 ppm, Ag^{+} removal rates remained >99.9% while Cu^{2+} removal rates decreased from 99.80% to 11.38%. The separation factor (SF) is used to indicate the ability to separate two substances and the SF >100 is thought to have good separation effect. As the molar ratio of Cu^{2+}/Ag^{+} ($n(Cu^{2+})/n(Ag^{+})$) increased, the $SF_{Ag/Cu}$ (K_d^{Ag}/K_d^{Cu}) also increased (Figure 2a,b). The nearly quantitative removal of Ag^{+} at whatever high Cu^{2+} concentration indicates the superior capture of Ag^{+} by Mo_3S_{13}-LDH. At the Cu/Ag ppm ratio ≥25:1, the $SF_{Ag/Cu}$ was larger than 770. At the higher ppm ratio of 520:1, the $SF_{Ag/Cu}$ reached an extremely large value of ≈8000.

Adsorption Isotherm and Uptake Capacity

During adsorption equilibrium study, we found the amount of Ag^{+} captured by Mo_3S_{13}-LDH increased with increasing initial ion concentrations (100–1700 ppm, Table 3). Over the initial concentration of ≈100–1000 ppm, the Ag^{+} removals reached ≥95%. The maximum adsorption capacity (q_m) of Ag^{+} achieved 1073 mg g^{-1}, giving an exceptionally high value exceeding reported top sorbents (Table 4).[7,11,16a,17,24] For Hg^{2+}, maximum adsorption capacity reached 594 mg g^{-1} (Table S3), which is also superior compared with the known sorbents listed in Table 4. All these illustrate the outstanding adsorption capacity of Mo_3S_{13}-LDH for Ag^{+} and Hg^{2+}.

Equilibrium adsorptions were fitted using isothermal equations of Langmuir and Freundlich (see Supporting Information). Langmuir model assumes the monolayer adsorption of sorbate onto sorbent surface, while Freundlich model is based on multilayered adsorption. From Figure 2c,d and Figure S1a,S1b, we observe the data points agree well with the Langmuir model ($R^2=0.997$), yielding a q_m of 1063 mg g^{-1} (see Table S4), close to the experimental value of 1073 mg g^{-1}, suggesting monolayer adsorption on the Mo_3S_{13}-LDH.

Adsorption Kinetics Study

Adsorption kinetics depicted the adsorption rates for Hg^{2+} and Ag^{+} were very fast (see Table 5). Within 10 min,

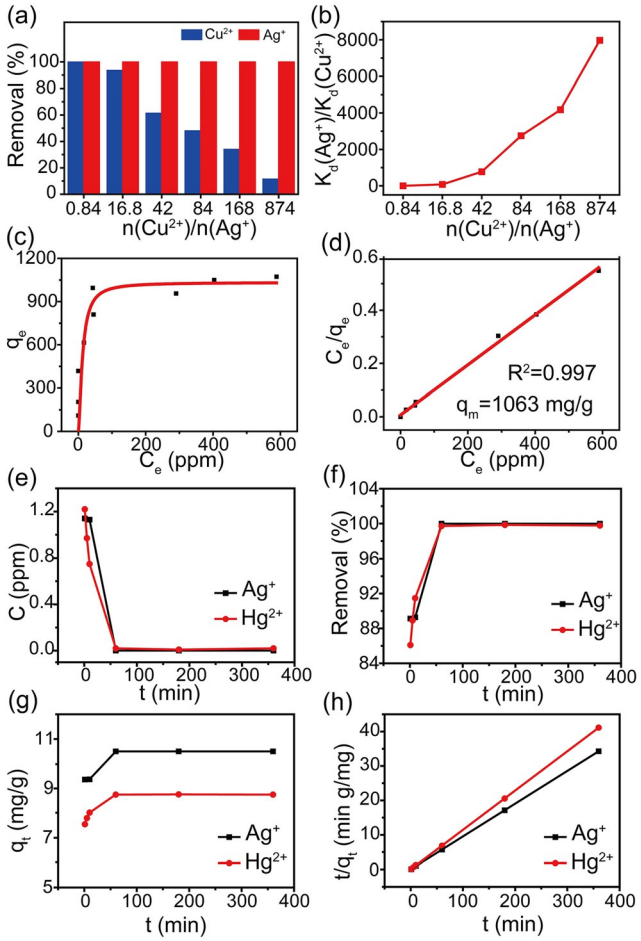

Figure 2. Selectivity towards Ag^+ and Cu^{2+} by Mo_3S_{13}-LDH: a) bar graph of removal rates and b) plots of $SF_{Ag/Cu}$ (K_d^{Ag}/K_d^{Cu}) as a function of $n(Cu^{2+})/n(Ag^+)$; c) Langmuir equilibrium isotherm of Ag^+ and d) linear form; kinetics curves for Ag^+ and Hg^{2+}: e) concentration change following contact time, f) removal% as a function of contact time, g) sorption capacity (q_t) with time, h) pseudo-second-order kinetic plots.

Table 3: Sorption data of Mo_3S_{13}-LDH toward Ag^+ in different concentrations.[a]

C_0 [ppm]	C_f [ppm]	pH	Removal [%]	q_m [mg g^{-1}]
110	0.002	5.22→4.53	99.99	110
205	0.007	5.20→4.46	99.99	205
418	0.001	5.26→4.22	99.99	418
632	16.4	5.34→3.94	97.40	615
855	45.0	4.91→3.97	94.70	810
1038	42.8	5.06→3.80	95.90	995
1246	290.1	5.21→3.85	76.70	956
1453	403.3	5.56→3.81	72.20	1050
1662	588.7	5.69→3.77	64.60	1073

[a] Contact time: 24 h, $V=20$ mL, $m=0.02$ g, $V/m=1000$ mL g^{-1}.

≈90% removal rates and ≈10^4 mL g^{-1} K_d were achieved for Hg^{2+} and Ag^+. Within 60 min, the removal rates reached ≥99.5% and K_d values got $>10^7$ mL g^{-1} for Ag^+ and $>10^5$ mL g^{-1} for Hg^{2+}. To get better understanding of adsorption rate and rate-controlling step, pseudo-first-order and pseudo-second-order models (see Supporting Information) are used to fit the experimental data.[25] The first-order kinetics is related to physical adsorption, whose sorption rate is controlled by concentration gradient of the sorbate.[26] The second-order kinetics is independent of concentration and normally corresponds to chemical adsorption.

Figure 2e–h demonstrates kinetics curves for Ag^+ and Hg^{2+}, with kinetic parameters listed in Table S5. The fitting results show that the correlation coefficient (R^2) of pseudo second-order kinetics is close to 1, so the adsorption process can be well described by a pseudo-second order model, suggesting the chemisorption. In this case, the rate of adsorption mainly depends on the driving force,[27] and the formation of strong metal-sulfur bonds provides powerful driving force beneficial to fast adsorption kinetics.[28] According to soft and hard acid-base theory, the S as a soft Lewis base would have strong affinity for the soft Lewis acids Ag^+ and Hg^{2+}. This results in strong binding and a large adsorption driving force. Simultaneously, the dispersed $Mo_3S_{13}^{2-}$ clusters in the LDH gallery provide multiple reactive sites for effective adsorption. In Table 4, we list the equilibrium time and k_2 values of the Mo_3S_{13}-LDH and other reported sorbents. These values indicate Mo_3S_{13}-LDH is a superior adsorbent for the fast separation of toxic heavy metals and extraction of noble metals.

Regeneration and Reusability of Mo_3S_{13}-LDH

Considering the significance of reusability of adsorbent in practical applications, the Mo_3S_{13}-LDH was evaluated by cyclic experiments for 10 ppm Ag^+, Hg^{2+} and Cu^{2+} solutions. Common eluents are HNO_3, $NaNO_3$ and EDTA (ethylene diamine tetraacetic acid). Considering that the Mo_3S_{13}-LDH is an alkaline material, it is not suitable for acid elution. $NaNO_3$ has bad elution effect on Ag^+, Hg^{2+} and Cu^{2+} adsorbed on the sorbent. We selected 0.2 M EDTA as the complexing agent for heavy metals solutions as described in reported materials of LDH-$[Sn_2S_6]$[29] and Fe-MoS_4.[24b] The adsorption and desorption results are depicted in Figure S2. We observed the desorptions of Ag^+ and Hg^{2+} were very difficult, which was attributed to the strong interactions of S-Ag and S-Hg in the adsorption. For Ag^+, since it is reduced to elemental Ag^0 solid, and therefore its elution is not possible. Therefore, although the adsorption rates of Ag^+ and Hg^{2+} could reach 99.9%, their elution rates were only 0.4% and 1%, respectively. In contrast, EDTA had a certain adsorption effect on copper. The first removal rate of Cu^{2+} achieved with 98.5% and the corresponding elution rate was 52.7%. With the increase of recycling times, the adsorption rate gradually decreased, and after three cycles, the uptake rate was only 17.6%.

Application of Mo_3S_{13}-LDH in Actual Water Environment

In order to explore the practical application of Mo_3S_{13}-LDH in the removal of ultra-low concentrated metal ions in water systems especially drinking water, we studied the

Table 4: Adsorption performance of MgAl-Mo_3S_{13}-LDH and reported adsorbents for metal ions.

Ions	adsorbents	q_m [mg g^{-1}]	Equilibrium time [min]	k_2 [g mg^{-1} min^{-1}]	Refs
Ag^+	**MgAl-Mo_3S_{13}-LDH**	**1063**	**60**	**0.2**	**this work**
	MgAl-Mo_3S_{13}-Ppy[a]	408	60	0.17	[11]
	MgAl-MoS_4-LDH[b]	450	30	2.24	[17]
	MoS_4-Ppy[c]	480	30	0.0083	[24a]
	MgAl-S_x-LDH[d]	383	180	–	[16a]
	KMS-2[e]	408	180	–	[7]
	Fe-MoS_4[f]	565	180	0.0009	[24b]
Hg^{2+}	**MgAl-Mo_3S_{13}-LDH**	**594**	**60**	**0.27**	**this work**
	MgAl-MoS_4-LDH	500	180	0.362	[17]
	KMS-2	297	300	–	[7]
	PANI-PS[g]	148	–	–	[24c]
	KMS-1[h]	377	60	–	[24d]
	LHMS-1[i]	87	–	–	[24e]
	Fe-MoS_4	582	180	0.001	[24b]

[a] MgAl-LDH intercalated with $Mo_3S_{13}^{2-}$. [b] MgAl-LDH intercalated with MoS_4^{2-}. [c] Polypyrrole (Ppy) functionalized with MoS_4^{2-}. [d] MgAl-LDH intercalated with polysulfide anions. [e] Layered metal sulfides of $K_{2x}Mg_xSn_{3-x}S_6$. [f] FeMgAl-LDH intercalated with MoS_4^{2-}. [g] olyaniline-polystyrene. [h] Layered metal sulfide $K_{2x}Mn_xSn_{3-x}S_6$. [i] Layered hydrogen metal sulfide (LHMS) of $H_{2x}Mn_xSn_{3-x}S_6$.

Table 5: Kinetics data of Ag^+ and Hg^{2+} adsorption by Mo_3S_{13}-LDH.

C_0 [ppm]	t [min]	C_f [ppm]	Removal [%]	q_t [mg g^{-1}]
10.5 (Ag^+)	1	1.14	89.14	9.36
	10	1.13	89.28	9.37
	60	0.001	99.99	10.50
	180	0.001	99.99	10.50
	360	0.001	99.99	10.50
8.77 (Hg^{2+})	1	1.22	86.09	7.55
	5	0.97	88.92	7.80
	10	0.75	91.48	8.02
	60	0.02	99.72	8.75
	180	0.01	99.84	8.76
	360	0.02	99.78	8.75

$V = 20$ mL, $m = 0.02$ g, $V/m = 1000$ mL g^{-1}.

Table 6: Adsorption of Mo_3S_{13}-LDH for heavy metal ions in two actual water environments.[a]

Sample	Metal ions	C_0 [ppb]	C_f [ppb]	Removal [%]	K_d [mL g^{-1}]
Mudanyuan area	Ag^+	ND	ND	–	–
	Hg^{2+}	0.26	0.05	80.77	4.2×10^3
	Cu^{2+}	0.45	0.26	42.22	731
	Pb^{2+}	ND	ND	–	–
Yuyuantan area	Ag^+	ND	ND	–	–
	Hg^{2+}	0.37	0.05	86.49	6.4×10^3
	Cu^{2+}	0.86	0.54	37.21	593
	Pb^{2+}	ND	ND	–	–

[a] Contact time: 24 h, $V = 20$ mL, $m = 0.02$ g, $V/m = 1000$ mL g^{-1}.

capture performance of Ag^+, Hg^{2+}, Cu^{2+} and Pb^{2+} in the river water of Beijing (Mudanyuan and Yuyuantan areas, whose exact location please see Supporting Information). As shown in Table 6, the concentrations of Ag^+ and Pb^{2+} in both Yuyuantan and Mudanyuan are very low, so ICP-MS had not detected their concentration. The concentrations of Hg^+ in both Mudanyuan and Yuyuantan were as low as only 0.26 and 0.37 ppb (μg L^{-1}), while the removal rates of Hg^+ could still reach 80.77 % and 86.49 %, respectively. For Cu^{2+}, under ultra-low concentrations of 0.45 and 0.86 ppb (μg L^{-1}), the removal effect was not as good as for Hg^{2+}, while the removal rates of 42.22 % and 37.21 % were achieved, showing that the capture for trace amount of copper ions was still effective. Thus, this sorbent can be used for the removal of $Cu^{2+}$and Hg^{2+} at trace level in actual water environment treatment. This indicates the Mo_3S_{13}-LDH would work as a promising adsorbent for the preparation of ultrapure water.

Characterization of Post-Adsorption Samples and Reaction Mechanism Analysis

At a fixed low concentration of ≈1 ppm of Ag^+ while varied concentrations (1–100 ppm) of Cu^{2+}, the post-adsorption solids showed similar XRD patterns, with the 0.91 nm d_{basal} (Figure 3 A) close to that of Mo_3S_{13}-LDH precursor, because the adsorbed amount was not large enough to create a new phase as observed in XRD. Also, there was no significant change in IR spectra (Figure 3 B). For Ag^+ at different concentrations (10–1000 ppm), the post-adsorption samples depicted different XRD patterns (Figure 3 C). At the low Ag^+ concentration of 10 ppm, a layered phase with the d_{basal} of 0.89 nm was observed (Figure 3 C-b). In this case, the $Mo_3S_{13}^{2-}$ cluster may coordinate with Ag^+ forming certain anionic complexes of $[Ag_x(Mo_3S_{13})_y]^{n-}$ arranging in the LDH gallery, together with the entered NO_3^-, resulting in shorter d_{basal}. At a higher Ag^+ concentration such as 100 ppm, in addition to the 0.89 nm phase (Figure 3 C-c), there appeared weak diffraction peaks which can be assigned to Ag_2S.[11] At 400 ppm Ag^+, the layered phase became invisible (Figure 3 C-d), and diffractions of metallic Ag^0 appeared besides the Ag_2S. From the SEM image (Figure 3 E), the post-adsorption sample (400 ppm Ag^+) still retained the hexagonal sheet morphology, although diffractions related to layered phase were undetectable by XRD. Similar hexagonal morphology was observed in the 400 ppm Hg^{2+}-adsorbed sample (Figure 3 F), depicting general preservation of laminate structure during adsorption of Hg^{2+}. At much higher silver concentration of 1000 ppm, metallic Ag^0 phase became much explicit and Ag_2S phase still existed (Figure 3 C-e). For clarity, we measured the XRD patterns of the 1000 ppm Ag-adsorbed sample at a low scan rate (Figure 3 D), and the X-ray

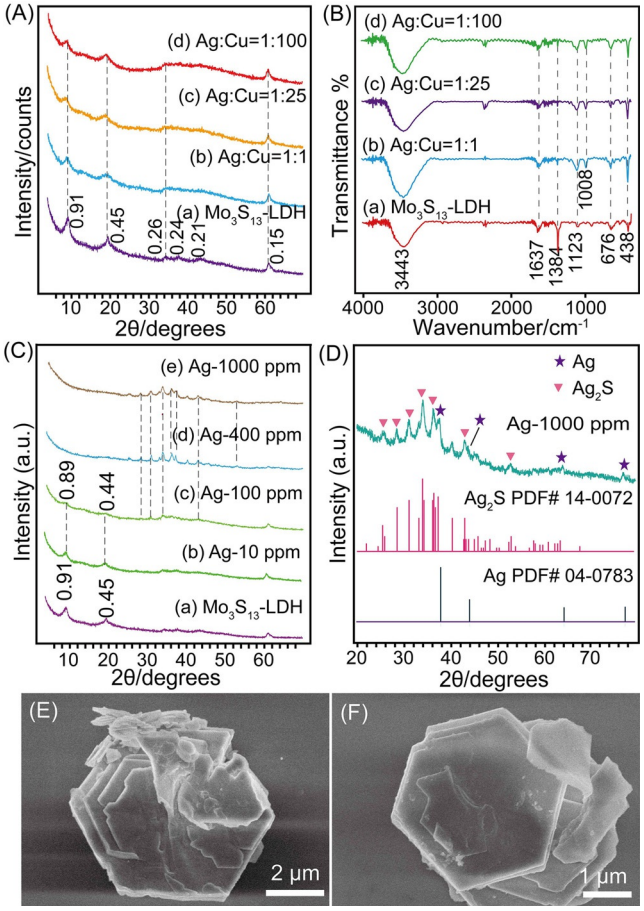

Figure 3. A) XRD patterns and B) IR spectra of solid samples before and after Mo_3S_{13}-LDH adsorbed Cu^{2+}/Ag^+ mixtures with different ratios; C) XRD patterns before and after Mo_3S_{13}-LDH adsorbed 100, 400, and 1000 ppm Ag^+; D) 1000 ppm Ag-adsorbed sample (at slow scan rate) and standard XRD patterns of Ag^0 and Ag_2S. SEM images of the post-adsorption samples after Mo_3S_{13}-LDH adsorbed E) 400 ppm Ag^+ and F) 400 ppm Hg^{2+}.

diffractions of Ag^0 and Ag_2S phases were also shown for reference.

Most importantly and surprisingly, during adsorption of highly concentrated Ag^+ such as 1200 ppm, we observed formation of large amount of metallic Ag. Figure 4a illustrates a Ag^0-containing sample in a beaker, where a rather slim silver thread and spherical aggregates mixed in the solid adsorbent are observed. The SEM images in Figure 4b-i, show large amount of Ag^0 with a clear ribbon structure. With increasing magnification (Figure 4 f-i), it is clear that metallic Ag^0 grew into large ribbons with lengths in the hundreds of μm, widths of ≈10 μm, and thicknesses of several nm.

To study the formation mechanism of elemental Ag^0, X-ray photoelectron spectroscopy (XPS) analyses were carried out to check the valence state change of the relevant elements particularly Mo. For pure $(NH_4)_2Mo_3S_{13}$ (Figure S3), the Mo exits as single valence state of +4, with the only two peaks with 232.5 and 229.2 eV related to $3d_{3/2}$ and $3d_{5/2}$ of Mo^{4+}. For 800 ppm Ag^+ post-adsorption sample, in addition to 232.7 and 229.6 eV peaks of Mo^{4+}, there appear the peaks at 235.6 and 232.7 eV which are ascribed to $3d_{3/2}$ and $3d_{5/2}$ of Mo in +6 valence, respectively, indicating the formation of oxidized Mo^{6+} (Figure 5a).[30] For 1300 ppm Ag^+-adsorbed sample (Figure 5b), the Mo^{4+} peaks $3d_{5/2}$ at 229.5 eV weaken further and the peaks at 232.6 and 235.6 eV for $3d_{5/2}$ and $3d_{3/2}$ of Mo^{6+} become stronger, indicating an increased amount of Mo^{6+}. For S 2p, in the $(NH_4)_2Mo_3S_{13}$, the energies in 165.0–163.0 eV are assigned to S_2^{2-} group while the two energies of 163.1 and 161.9 eV are ascribed to the S^{2-} group. In the 800 ppm Ag^+ post-adsorption sample, the amount of S_2^{2-} (with energies of 164.4–162.5 eV) is significantly reduced relative to that of the S^{2-} (with energies of 162.5–161.3 eV), as shown in Figure 5a″. And with the increased Ag^+ concentration of 1300 ppm (Figure 5b′), the amount of S_2^{2-} is continually reduced, which suggests the S_2^{2-} ions react and are oxidized possibly converting to soluble SO_4^{2-} (should go into solution). At the same time, the peak of Ag 3d at 368.3 eV ascribed to metallic Ag (Figure 5a″, b″).[31]

Mo in the post-adsorption solids is mainly in the +6 valence, implying the presence of MoS_4^{2-}, MoO_4^{2-} or MoO_3. For the oxidation of sulfur of S_2^{2-}, it may become elemental S^0 or SO_4^{2-}. Therefore, we put forward three possible reactions as below:

$$Mo_3S_{13}^{2-} + 50\,Ag^+ + 32\,H_2O \rightarrow 8\,Ag_2S + 5\,SO_4^{2-} + 3\,MoO_4^{2-} + 34\,Ag^0 + 64\,H^+ \quad (1)$$

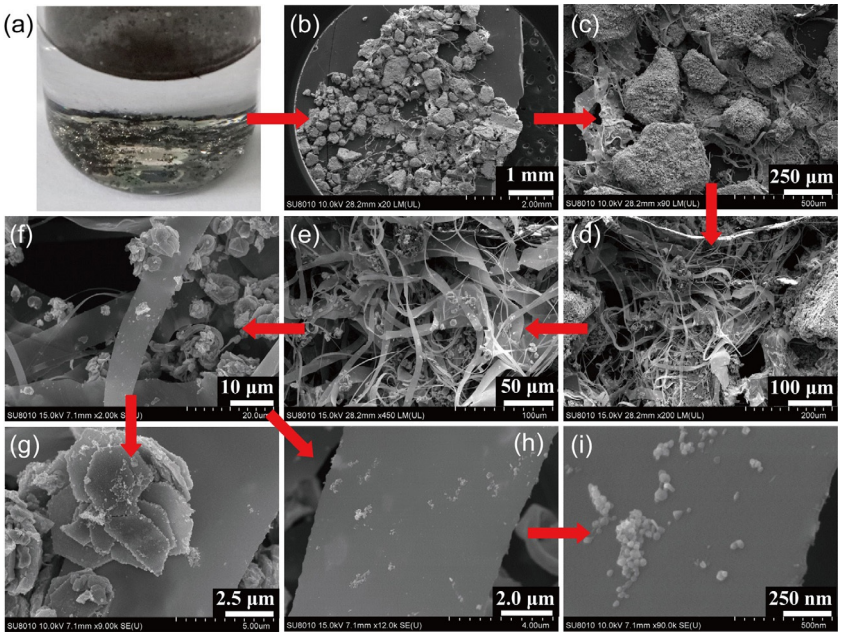

Figure 4. a) Digital photo of Mo_3S_{13}-LDH absorbed 1200 ppm Ag^+ in a beaker. b)–i) SEM images of solid samples after Mo_3S_{13}-LDH absorbed 1200 ppm Ag^+. Different image magnifications clearly show the morphology, shape and size of the formed Ag^0.

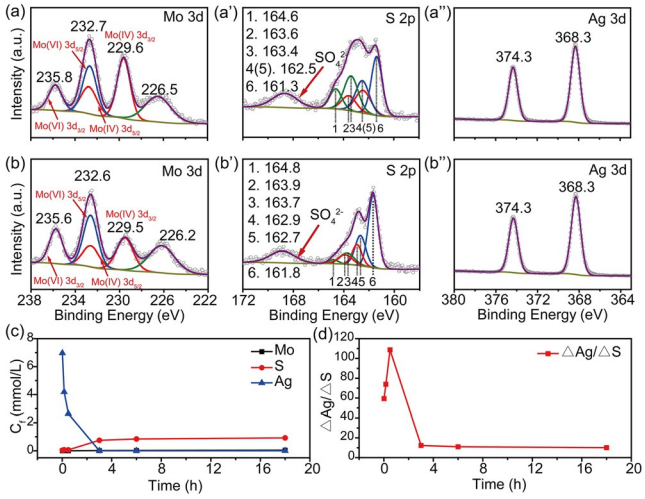

Figure 5. XPS spectra of solid samples after Mo_3S_{13}-LDH adsorbed a)–a″) 800 ppm Ag^+ and b)–b″) 1300 ppm Ag^+; c) Concentration change of Ag, Mo, and S with the contact time (initial Ag^+ concentrations is 1000 ppm, $V/m = 20$ mL/0.02 g = 1000 mL g^{-1}); d) Relationship of mole ratio of the reduced Ag (ΔAg) to increased S (ΔS), that is ΔAg/ΔS, with the contact time.

$$Mo_3S_{13}^{2-} + 20\,Ag^+ + 9\,H_2O \rightarrow 7\,Ag_2S + 6\,S^0 + 3\,MoO_3 + 6\,Ag^0 + 18\,H^+ \quad (2)$$

$$Mo_3S_{13}^{2-} + 50\,Ag^+ + 29\,H_2O \rightarrow 8\,Ag_2S + 5\,SO_4^{2-} + 3\,MoO_3 + 34\,Ag^0 + 58\,H^+ \quad (3)$$

For the redox reaction, the direction of the reaction could be determined by its reaction electromotive force (E), which can be obtained from the standard redox potential (E_0) of different redox pairs. The E values are associated with the thermodynamics feasibility of the reaction. The $Mo_3S_{13}^{2-}$ consists of S_2^{2-}, S^{2-}, and Mo^{4+}, in which S_2^{2-} and Mo^{4+} participate in the reduction of Ag^+ to Ag^0. The S_2^{2-} involves in the reduction to S^{2-} ($E_0(S_2^{2-}/S^{2-}) = 0.34$ V)[32] and oxidation to S^0 or SO_4^{2-}. The $E_0(SO_4^{2-}/S_2^{2-})$ of 0.334 V or $E_0(S^0/S_2^{2-})$ of −0.20 V vs. $E_0(Ag^+/Ag^0)$ of 0.80 V means a positive E value, inferring the thermodynamics is feasible. However, the $E_0(MoO_4^{2-}/MoO_2)$ of 0.65 V[33] vs. $E_0(Ag^+/Ag^0)$ of 0.80 V also corresponds to a positive E value, showing it is thermodynamically feasible.[34] Further, we can evaluate the feasibility of the proposed reactions (1–3) by estimating the approximate minimum E values (E_{min}). From the calculated results we found the three equations have positive E values (for details of calculations see Supporting Information), suggesting all of these processes are rational from the thermodynamics point of view.

From the three reactions above, (1) gives soluble products of both Mo and S (MoO_4^{2-} and SO_4^{2-}), (2) gives insoluble elemental S^0 and MoO_3, and (3) gives soluble S product (SO_4^{2-}) while insoluble MoO_3. To find out which reaction is more representative of the system, we designed Ag adsorption experiments under different contact times and detected the reduced amount of Ag and increased amount of S (and/or Mo) if released into the solution by ICP. From Table S6 and Figure 5c,d, we found with increasing contact time, the concentration of Ag decreased and the concentrations of S increased. Although Mo in the solution was also detected and its concentration was increased, the Mo amount was very low compared with S, with S/Mo ratios of 12–62 (Table S6) which are much larger than the values of 1.7–2 (5:3–6:3) from reactions (1)–(3). So we think the Mo released into the solution is negligible. Thus we can rule out the reaction (1). For reaction (2), the insoluble S in water also cannot account for the significant S detected in the solution, so we also rule out this process. When the adsorption achieves an equilibrium, the mole ratio of the reduced Ag (ΔAg) to the increased S (ΔS), that is $\Delta Ag/\Delta S$, is equal to ≈ 10. This matches well with the tested ΔAg/ΔS ratio of 10.06 (at 18 h contact time) and the insoluble MoO_3 also accounts for why only a trace of Mo is detected in the solution. From Table S6 and Figure 5c,d, the $\Delta Ag/\Delta S$ went up first and then went down. The relatively high $\Delta Ag/\Delta S$ ratio in the initial stage means low S content released into the solution. This suggests that in the early stage of the adsorption, the decreased Ag did not result in corresponding increase of S in the solution, suggesting that insoluble Ag_2S is dominant product which is obtained by precipitation. In the later stage, oxidation-reduction reaction dominates, with the formation of metallic Ag^0, and the S_x^{2-} species are oxidized to SO_4^{2-} which then release into the solution. So at this time, the detected S amount in solution increases markedly and the ΔAg/ΔS decreases greatly. According to these results, we deduce the reaction mechanism relies on reaction (3) where the $Mo_3S_{13}^{2-}$ cluster acts as a tremendous reservoir of donated electrons.

Here we advance a physical explanation for the observed dual role of Mo_3S_{13}-LDH in simultaneously forming Ag_2S and reducing Ag^+ ions. As known the $Mo_3S_{13}^{2-}$ cluster consists of one S^{2-}, six S_2^{2-}, and three Mo^{4+}, all of which participate in the reaction with Ag^+. When it contacts Ag^+, the $Mo_3S_{13}^{2-}$ reacts with Ag^+ and breaks down quickly. The one S^{2-} will react directly with two Ag^+ to form one equivalent of Ag_2S, while the S_2^{2-} take part in the reduction to S^{2-} and oxidation to S^0 or SO_4^{2-} (a disproportionation reaction). The reduced product of S^{2-} ions will react with Ag^+ to form other Ag_2S. For oxidation product of S_2^{2-}, from our proposed reaction (3), we know experimentally its should be SO_4^{2-} but not S^0. With the oxidation of S_2^{2-} to SO_4^{2-}, the Ag^+ is reduced to Ag^0. In addition, the Mo^{4+} can also reduce the Ag^+ to Ag^0 and the Mo^{4+} by itself is oxidized to form stable MoO_3. All these reactions contribute to the concomitant reduction of Ag^+ to Ag^0 and formation of Ag_2S.

Figure 6 depicts the sorption mechanism of Mo_3S_{13}-LDH for heavy metal ions especially Ag^+: (1) at low content of Ag^+, where the Mo_3S_{13}-LDH is in large excess, Ag^+ ions coordinate with $Mo_3S_{13}^{2-}$ to form $[Ag_x(Mo_3S_{13})_y]^{n-}$ anions which remain in the LDH interlayers (Figure 6a); (2) when Ag^+ ions are in medium quantities, Ag_2S and Ag^0 nanoparticles would be formed via oxidation-reduction reactions of $Mo_3S_{13}^{2-}$ with Ag^+ (Figure 6b); (3) when Ag^+ ions are in large excess, nanosized Ag metals grow into large size to form ribbons, coexisting with the Ag_2S (Figure 6c); (4) for other heavy metal ions of Hg^{2+} and Cu^{2+}, the adsorption mechanism may be similar to that of low concentrated Ag^+ (Figure 6d).

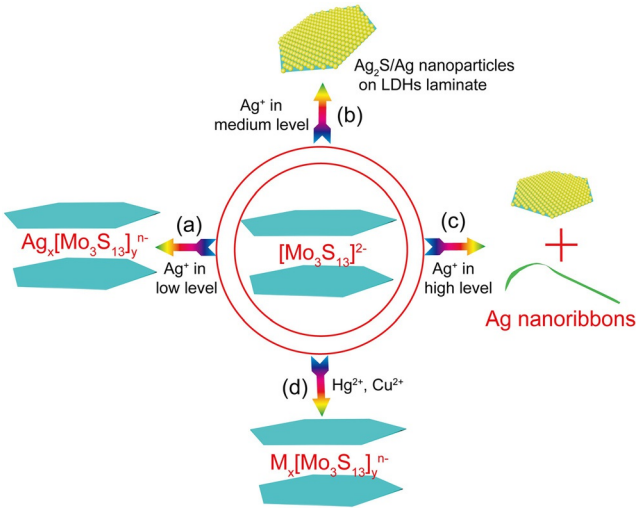

Figure 6. Possible sorption mechanism during Mo_3S_{13}-LDH adsorbing heavy metal ions of Ag^+, Cu^{2+}, and Hg^{2+}.

Conclusion

The Mo_3S_{13}-LDH can be prepared via insertion of $Mo_3S_{13}^{2-}$ into LDH interlayers and exhibits excellent uptake and selectivity for the heavy metal ions of Cu^{2+}, Hg^{2+}, and Ag^+. The key findings are: (a) the Mo_3S_{13}-LDH achieves extremely high adsorption capacities for Ag^+ ($\approx$1073 mg g^{-1}) and Hg^{2+} (598 mg g^{-1}); (b) the Mo_3S_{13}-LDH exhibits ultra fast adsorption for Ag^+ and Hg^{2+} and the fitted pseudo-second-order kinetics model indicates a chemisorption associated with formation of strong metal-sulfur bonding; (c) outstanding separation capability of trace amounts of Ag^+ in the presence of highly concentrations of Cu^{2+} enables efficient extraction of Ag from low-grade minerals; (d) the reduction capability of Mo^{4+} and S_x^{2-} in Mo_3S_{13}-LDH makes the successful acquisition of elemental Ag^0 from complex Ag^+-containing solutions. All these advantages make the Mo_3S_{13}-LDH material promising for decontamination of water polluted by heavy metal ions and for the extraction of silver as a precious metal from a variety of aqueous sources.

Acknowledgements

This work is supported by National Natural Science Foundation of China (No. U1832152 and 22176017), Ningxia Key research and Development Program (No. 2018BEG03017), Natural Science Foundation of Ningxia (2020AAC03115), China Postdoctoral Science Foundation (2020M680430), Foundation of State Key Laboratory of High-efficiency Utilization of Coal and Green Chemical Engineering (No. 2020-KF-40). At Northwestern University this work was partially supported by National Science Foundation Grant DMR-2003476.

Conflict of Interest

The authors declare no conflict of interest.

Keywords: heavy metal removal · layered double hydroxides · mercury · Mo_3S_{13}-LDH material · silver extraction

[1] a) V. Chandra, K. S. Kim, *Chem. Commun.* **2011**, *47*, 3942 – 3944; b) H. Asiabi, Y. Yamini, M. Shamsayei, E. Tahmasebi, *Chem. Eng. J.* **2017**, *323*, 212 – 223; c) R. Shawabkeh, A. Al-Harahsheh, A. Al-Otoom, *Sep. Purif. Technol.* **2004**, *40*, 251 – 257.
[2] a) A. H. Alshehri, M. Jakubowska, A. Mlozniak, M. Horaczek, D. Rudka, C. Free, J. D. Carey, *ACS Appl. Mater. Interfaces* **2012**, *4*, 7007 – 7010; b) W. B. Luo, X. W. Gao, S. L. Chou, J. Z. Wang, H. K. Liu, *Adv. Mater.* **2015**, *27*, 6862 – 6869; c) J. Lu, L. Cheng, K. C. Lau, E. Tyo, X. Luo, J. Wen, D. Miller, R. S. Assary, H. H. Wang, P. Redfern, H. Wu, J. B. Park, Y. K. Sun, S. Vajda, K. Amine, L. A. Curtiss, *Nat. Commun.* **2014**, *5*, 4895; d) C. Wu, T. W. Kim, T. Guo, F. Li, *Nano Energy* **2017**, *32*, 367 – 373; e) J. Thiel, L. Pakstis, S. Buzby, M. Raffi, C. Ni, D. J. Pochan, S. I. Shah, *Small* **2007**, *3*, 799 – 803; f) M. Liong, B. France, K. A. Bradley, J. I. Zink, *Adv. Mater.* **2009**, *21*, 1684 – 1689.
[3] P. Wang, N. W. Menzies, P. G. Dennis, J. Guo, C. Forstner, R. Sekine, E. Lombi, P. Kappen, P. M. Bertsch, P. M. Kopittke, *Environ. Sci. Technol.* **2016**, *50*, 8274 – 8281.
[4] S. J. Billinge, E. J. McKimmy, M. Shatnawi, H. Kim, V. Petkov, D. Wermeille, T. J. Pinnavaia, *J. Am. Chem. Soc.* **2005**, *127*, 8492 – 8498.
[5] M. J. Manos, N. Ding, M. G. Kanatzidis, *Proc. Natl. Acad. Sci. USA* **2008**, *105*, 3696 – 3699.
[6] M. J. Manos, M. G. Kanatzidis, *J. Am. Chem. Soc.* **2009**, *131*, 6599 – 6607.
[7] Z. Hassanzadeh Fard, C. D. Malliakas, J. L. Mertz, M. G. Kanatzidis, *Chem. Mater.* **2015**, *27*, 1925 – 1928.
[8] D. Sarma, C. D. Malliakas, K. S. Subrahmanyam, S. M. Islam, M. G. Kanatzidis, *Chem. Sci.* **2016**, *7*, 1121 – 1132.
[9] Z. Hassanzadeh Fard, S. M. Islam, M. G. Kanatzidis, *Chem. Mater.* **2015**, *27*, 6189 – 6192.
[10] J. Kibsgaard, T. F. Jaramillo, F. Besenbacher, *Nat. Chem.* **2014**, *6*, 248 – 253.
[11] M. Yuan, H. Yao, L. Xie, X. Liu, H. Wang, S. M. Islam, K. Shi, Z. Yu, G. Sun, H. Li, S. L. Ma, M. G. Kanatzidis, *J. Am. Chem. Soc.* **2020**, *142*, 1574 – 1583.
[12] a) F. Chen, F. Hou, L. Huang, J. Cheng, H. Liu, P. Xi, D. Bai, Z. Zeng, *Dyes Pigm.* **2013**, *98*, 146 – 152; b) X. Y. Xue, Q. Y. Gu, G. H. Pan, J. Liang, G. L. Huang, G. B. Sun, S. L. Ma, X. J. Yang, *Inorg. Chem.* **2014**, *53*, 1521 – 1529; c) S. L. Ma, C. H. Fan, L. Du, G. L. Huang, X. J. Yang, W. P. Tang, Y. Makita, K. Ooi, *Chem. Mater.* **2009**, *21*, 3602 – 3610.
[13] a) V. R. Constantino, T. J. Pinnavaia, *Catal. Lett.* **1994**, *23*, 361 – 367; b) A. Corma, V. Fornes, F. Rey, A. Cervilla, E. Llopis, A. Ribera, *J. Catal.* **1995**, *152*, 237 – 242.
[14] Z. Gao, J. Wang, Z. Li, W. Yang, B. Wang, M. Hou, Y. He, Q. Liu, T. Mann, P. Yang, M. Zhang, L. Liu, *Chem. Mater.* **2011**, *23*, 3509 – 3516.
[15] A. I. Khan, D. O'Hare, *J. Mater. Chem.* **2002**, *12*, 3191 – 3198.
[16] a) S. L. Ma, Q. Chen, H. Li, P. Wang, S. M. Islam, Q. Gu, X. Yang, M. G. Kanatzidis, *J. Mater. Chem. A* **2014**, *2*, 10280 – 10289; b) S. L. Ma, L. Huang, L. Ma, Y. Shim, S. M. Islam, P. Wang, L. D. Zhao, S. Wang, G. Sun, X. Yang, M. G. Kanatzidis, *J. Am. Chem. Soc.* **2015**, *137*, 3670 – 3677.
[17] L. J. Ma, Q. Wang, S. M. Islam, Y. C. Liu, S. L. Ma, M. G. Kanatzidis, *J. Am. Chem. Soc.* **2016**, *138*, 2858 – 2866.
[18] L. Ma, S. M. Islam, H. Liu, J. Zhao, G. Sun, H. Li, S. L. Ma, M. G. Kanatzidis, *Chem. Mater.* **2017**, *29*, 3274 – 3284.

[19] L. Ma, S. Islam, C. Xiao, J. Zhao, H. Liu, M. Yuan, G. Sun, H. Li, S. Ma, M. G. Kanatzidis, *J. Am. Chem. Soc.* **2017**, *139*, 12745 – 12757.
[20] K. Vellingiri, K. H. Kim, A. Pournara, A. Deep, *Prog. Mater. Sci.* **2018**, *94*, 1 – 67.
[21] A. Müller, V. Wittneben, E. Krickemeyer, H. Bögge, M. Lemke, *Z. Anorg. Allg. Chem.* **1991**, *605*, 175 – 188.
[22] J. Lehto, A. Clearfield, *J. Radioanal. Nucl. Chem.* **1987**, *118*, 1 – 13.
[23] a) W. Yantasee, C. L. Warner, T. Sangvanich, R. S. Addleman, T. G. Carter, R. J. Wiacek, G. E. Fryxell, C. Timchalk, M. G. Warner, *Environ. Sci. Technol.* **2007**, *41*, 5114 – 5119; b) X. Chen, X. Feng, J. Liu, G. E. Fryxell, M. Gong, *Sep. Sci. Technol.* **1999**, *34*, 1121 – 1132.
[24] a) L. X. Xie, Z. H. Yu, S. M. Islam, K. R. Shi, Y. H. Cheng, M. W. Yuan, J. Zhao, G. B. Sun, H. F. Li, S. L. Ma, M. G. Kanatzidis, *Adv. Funct. Mater.* **2018**, *28*, 1800502; b) A. Jawad, Z. Liao, Z. Zhou, A. Khan, T. Wang, J. Ifthikar, A. Shahzad, Z. Chen, Z. Chen, *ACS Appl. Mater. Interfaces* **2017**, *9*, 28451 – 28463; c) J. J. Alcaraz-Espinoza, A. E. Chavez-Guajardo, J. C. Medina-Llamas, C. A. Andrade, C. P. de Melo, *ACS Appl. Mater. Interfaces* **2015**, *7*, 7231 – 7240; d) M. J. Manos, M. G. Kanatzidis, *Chem. Eur. J.* **2009**, *15*, 4779 – 4784; e) M. J. Manos, V. G. Petkov, M. G. Kanatzidis, *Adv. Funct. Mater.* **2009**, *19*, 1087 – 1092.
[25] T. Liu, M. Yang, T. Wang, Q. Yuan, *Ind. Eng. Chem. Res.* **2012**, *51*, 454 – 463.
[26] J. P. Simonin, *Chem. Eng. J.* **2016**, *300*, 254 – 263.
[27] Y. Ho, A. Ofomaja, *J. Hazard. Mater.* **2006**, *129*, 137 – 142.
[28] Y. S. Ho, G. McKay, *Process Biochem.* **1999**, *34*, 451 – 465.
[29] A. Celik, D. R. Baker, Z. Arslan, X. Zhu, A. Blanton, J. Nie, S. Yang, S. Ma, F. X. Han, S. M. Islam, *Chem. Eng. J.* **2021**, *426*, 131696.
[30] V. Rives, M. A. Ulibarri, *Coord. Chem. Rev.* **1999**, *181*, 61 – 120.
[31] P. Liu, J. Liu, S. Cheng, W. Cai, F. Yu, Y. Zhang, P. Wu, M. Liu, *Chem. Eng. J.* **2017**, *328*, 1 – 10.
[32] J. Ali, A. Shahzad, J. Wang, J. Ifthikar, W. Lei, G. G. Aregay, Z. Chen, Z. Chen, *Chem. Eng. J.* **2021**, *408*, 127242.
[33] Y. Yu, L. Lu, Q. Yang, A. Zupanic, Q. Xu, L. Jiang, *ACS Appl. Nano Mater.* **2021**, *4*, 7523 – 7537.
[34] J. Ali, L. Wenli, A. Shahzad, J. Ifthikar, G. G. Aregay, I. I. Shahib, Z. Elkhlifi, Z. Chen, Z. Chen, *Water Res.* **2020**, *181*, 115862.

Manuscript received: September 14, 2021
Accepted manuscript online: October 28, 2021
Version of record online: November 23, 2021